Intranasal Anti-CD3 Antibody Treatment Attenuates Post–COVID Neuroinflammation and Enhances Hippocampal Neurogenesis and Cognitive Function in Mice

Peiwen Lu[1,*], Saef Izzy[2,3,4*&], Patrick Da Silva[2,3], Harm Tjebbe Imkamp[2,3,4], Jonathan R. Christenson[2,3,4], Taha Yahya[2,3,4], Maryam Hazim Al Mansi[2,3,4], Amir Alawi[2,3], Thais G. Moreira[3], Michelle Monje[5,6,7], Howard L. Weiner [3,&], Akiko Iwasaki[1,8,&]

[*]Equal contribution

[&]co-corresponding, equal contribution

Affiliations:

1. Department of Immunobiology, Yale University, New Haven CT USA
2. Immunology of Brain Injury Program, Brigham & Women's Hospital, Harvard Medical School, Boston, MA, USA
3. Ann Romney Center for Neurologic Diseases, Brigham & Women's Hospital, Harvard Medical School, Boston, MA, USA
4. Divisions of Stroke, Cerebrovascular, and Critical Care Neurology, Department of Neurology, Brigham and Women's Hospital, Harvard Medical School, Boston, MA, USA
5. Department of Neurology and Neurological Sciences, Stanford University, Stanford, CA, USA
6. Department of Pathology, Stanford University, Stanford, CA, USA
7. Howard Hughes Medical Institute, Stanford University, Stanford, CA, USA
8. Howard Hughes Medical Institute, Yale University, New Haven CT USA

Correspondence:
Akiko Iwasaki, PhD
akiko.iwasaki@yale.edu
Howard L. Weiner, MD
hweiner@bwh.harvard.edu
Saef Izzy, MD
sizzy@bwh.harvard.edu

Keywords: mild COVID-19, cognitive impairment, neuroinflammation, microglia, hippocampal neurogenesis, Treg, anti-CD3 therapy

Abstract:

Cognitive impairment is a disabling feature of Long COVID, with data supporting neuroinflammation and maladaptive glial responses as primary drivers. Nasal administration of an anti-CD3 monoclonal antibody (aCD3 mAb) has shown therapeutic benefits in autoimmune and CNS disease models. Using a respiratory-restricted mild SARS-CoV-2 mouse model of Long COVID, we show that nasal anti-CD3 mAb, administered shortly after infection or during chronic neuroinflammation, increased brain FoxP3+ IL–10+ Tregs, reduced microglial and astrocytic gliosis in the white matter and hippocampus, restored neurogenesis, and improved short-term memory. Nasal aCD3 mAb reprogrammed microglia from an antigen-presenting, NF-κB-driven inflammatory state toward chemokine signaling, phagosome, and TGF β–related regulatory phenotype. Patients with Long COVID with neurological symptoms had lower circulating Treg populations. These findings identify nasal administration of aCD3 mAb as a noninvasive strategy to control neuroinflammation, restore the neurogenic niche, and offer a novel approach to treating cognitive impairment in Long COVID.

48 **Introduction:**

49 Long COVID, or post-acute sequelae of SARS CoV-2 infection, is a heterogeneous syndrome in
50 which symptoms persist or recur months after the initial illness, typically beyond the period of
51 viral clearance (Groff et al., 2021; Nalbandian et al., 2021). Cognitive and neuropsychiatric
52 manifestations, including impaired attention, memory, and executive function that are commonly
53 described as 'brain fog,' together with fatigue and sleep disturbances, are among its most
54 debilitating features (Monje and Iwasaki, 2022; Xu et al., 2022). These symptoms can persist for
55 years, substantially limiting work capacity, daily functioning, and social participation, often in
56 adults during mid-life (Al-Aly et al., 2024; Davis et al., 2023). Understanding how post-viral CNS
57 dysfunction contributes is crucial, not only for persistent disability but also for processes
58 associated with brain aging, neurodegeneration, and increased vulnerability to cognitive decline in
59 later life decline in at-risk individuals(Bonhenry et al., 2024; Bruno et al., 2025; Seo et al., 2025).
60

61 However, the biological mechanisms linking respiratory viral infection to sustained cognitive
62 impairment remain poorly defined, and no approved therapies target the neurological
63 manifestations of Long COVID (Iwasaki and Putrino, 2023; Peluso and Deeks, 2024). Progress
64 has been hindered by two major challenges: the heterogeneous pathophysiology of Long COVID
65 and the lack of preclinical models that faithfully recapitulate persistent CNS dysfunction after
66 respiratory infection (Ellen, 2025; Hamlin and Blish, 2024; Jansen et al., 2022; Pagliano et al.,
67 2025), leaving clinical trials to proceed without clear biomarkers, patient stratification, or strong
68 mechanistic support. Available interventions also remain limited once symptoms are established.
69 Although vaccination attenuates acute disease severity and reduces the risk of developing Long
70 COVID by lowering infection (Green et al., 2025; Vanderheiden et al., 2024), protection is
71 incomplete, breakthrough infections still occur, and vaccination does not consistently alter the

severity or profile of neurological symptoms in individuals with established symptoms(Mukherjee et al., 2025; Notarte et al., 2022). These limitations underscore the need for mechanism-based therapies that directly target neuroimmune processes sustaining chronic CNS dysfunction.

Multiple studies indicate that SARS-CoV-2 infection can lead to sustained not only peripheral immune dysregulation(Yin et al., 2024) but also neuroinflammation, microglial reactivity, blood-brain barrier disruption, and impaired hippocampal neurogenesis in the CNS, even when acute infection is restricted to the respiratory tract(Braga et al., 2023; Fujimoto et al., 2025; Greene et al., 2024; Saikarthik et al., 2025). Experimental models of mild, respiratory-restricted SARS-CoV-2 infection recapitulates these features, revealing persistent microglial reactivity, white matter pathology, oligodendrocyte and myelin loss, as well as chemokine changes including elevated CCL11 that impair hippocampal neurogenesis and mirror alterations observed in people with Long COVID(Fernandez-Castaneda et al., 2022; Israelow et al., 2020).

Foxp3+ regulatory T (Treg) cells are a subset of CD4+ T cells that maintain immune homeostasis by restraining excessive effector responses and producing anti-inflammatory mediators such as IL-10 and TGF-β (Vignali et al., 2008). Across diverse neuroinflammatory and neurodegenerative conditions, Foxp3+ Treg cells have emerged as key regulators that limit CNS inflammation and support tissue repair, and their quantitative or functional impairment has been linked to worse neurological outcomes.(Liston et al., 2022; Liston et al., 2024). These observations suggest that augmenting Treg–mediated regulation could counteract the neuroinflammatory component of Long COVID and promote recovery of CNS function.

Mucosal delivery provides a physiologic, tolerogenic route for inducing regulatory T cell

96 responses and has shown a favorable safety profile in prior studies(Ochi et al., 2006; Weiner et al.,
97 2011). Nasal administration of anti-CD3 monoclonal antibody (aCD3 mAb) induces Treg
98 responses(Kuhn and Weiner, 2016; Wu et al., 2008) and has shown therapeutic benefit in both
99 autoimmune and CNS models of disease, including models of brain injury, progressive multiple
100 sclerosis (MS) and Alzheimer's disease (Izzy et al., 2025; Lopes et al., 2023; Mayo et al., 2016).
101 Nasal human aCD3 mAb is currently being investigated in clinical trials across several high-need
102 therapeutic areas, including MS and Alzheimer's disease(Chitnis et al., 2026; Singhal et al., 2025).
103 We therefore asked whether nasal aCD3 could influence outcomes in model of Long COVID by
104 modulating CNS immune responses.
105
106 Here, we used a validated mild COVID mouse model in which SARS-CoV-2 infection is restricted
107 to the respiratory tract yet leads to persistent CNS pathology that resembles the human Long
108 COVID phenotype. We show that nasal aCD3 induces Foxp3+ Treg cells that access the CNS,
109 reprogram microglia, reduce gliosis across affected regions, and restore hippocampal neurogenesis
110 and cognitive performance, thereby directly ameliorating Long COVID–like pathology. Together,
111 these findings identify nasal aCD3–mediated Treg induction as a mechanistically grounded,
112 immune-based strategy for treating Long COVID–associated neurological manifestations and,
113 more broadly, for targeting neuroinflammation in post-infectious brain disorders.
114
115

116 **Results:**

117 **Early nasal anti-CD3 mAb treatment limits neuroinflammatory changes in a Long COVID**
118 **mouse model**

119 To test whether aCD3 mAb can modify post-infectious CNS inflammation, we administered aCD3
120 mAb intranasally in a validated mild COVID model of respiratory-restricted SARS-CoV-2
121 infection (Figure 1A)(Fernandez-Castaneda et al., 2022). Although aCD3 engages the T cell
122 receptor complex (Chatenoud and Bluestone, 2007), 4 weeks of treatment did not alter anti–SARS
123 CoV-2 spike antibody titers, indicating that nasal anti-CD3 did not blunt the antiviral humoral
124 immunity (Figure S1A). We next quantified glial responses in brain regions implicated in post-
125 infectious cognitive dysfunction, including subcortical white matter and hippocampus. Infected
126 mice receiving isotype control showed a marked increase in IBA1+ microglia in both regions
127 compared with mock-infected animals, consistent with the previous report (Fernandez-Castaneda
128 et al., 2022)(Figure 1B). Nasal aCD3 substantially reduced microglial accumulation in each region,
129 restoring cell numbers toward mock levels (Figure 1B, S1B). We observed a similar pattern for
130 astrocytic gliosis. GFAP immunostaining revealed robust astrocyte reactivity in the subcortical
131 white matter and hippocampus of isotype-treated mild COVID mice (Eng et al., 1971; Hol and
132 Pekny, 2015), whereas aCD3 treatment significantly reduced GFAP+ astrocyte density across these
133 regions (Figure 1C). To determine whether these CNS changes were accompanied by systemic
134 immune modulation, we profiled circulating cytokines and chemokines. Nasal aCD3 decreased
135 serum CXCL10 and increased IL-10 relative to isotype treated mild COVID mice, consistent with
136 a shift toward a more regulatory immune milieu (Figure. 1D). Together, these data show that
137 initiating nasal aCD3 soon after acute SARS CoV-2 infection attenuates microglial and astrocytic
138 activation, prevents the establishment of chronic neuroinflammation and is associated with
139 systemic cytokine changes indicative of enhanced immune regulation.

140

141 **Early nasal anti-CD3 mAb reprograms microglial transcriptional states in the CNS**

142 To define how nasal aCD3 mAb reshapes microglial states after mild COVID, we performed bulk
143 RNA seq on subcortical microglia isolated from mock-infected mice and from mild COVID mice
144 treated with isotype control or nasal aCD3 mAb (Figure 2A, S1C, S1D). Compared with mock,
145 isotype-treated mild COVID mice showed extensive transcriptional reprogramming, with 209
146 differentially expressed genes (DEGs), whereas aCD3 treatment yielded 242 DEGs relative to
147 isotype, indicating a robust shift in the infection-primed microglial transcriptome (Figure 2B).
148 Analysis of genes that were significantly changed in both groups (mock versus isotype and aCD3
149 versus isotype) revealed a shared gene set that was strongly upregulated in microglia from isotype-
150 treated mild COVID mice but returned toward mock levels in anti–CD3–treated mice, indicating
151 that nasal aCD3 reverses an infection induced microglial activation program (Figure S1E)(Grant
152 et al., 2024). Analysis of the full microglial DEG set highlighted multiple biological programs
153 altered by infection and aCD3 treatment. This broader view included changes in immune-
154 associated features, including antigen processing and presentation genes (e.g., Cd74, H2-Ab1, H2-
155 K2) and chemokine/chemokine receptor-related genes (e.g., Ccl12, Ccr2) (Figure 2C). Gene
156 ontology analysis of DEGs shared across groups revealed enrichment for pathways related to
157 protein catabolism, autophagosome assembly and macrophage differentiation (Figure 2D). These
158 signatures suggested that post-infection aCD3 treatment influences not only inflammatory
159 signaling but also microglial phagocytic and structural interactions with myelinated axons. When
160 we focused specifically on genes upregulated by aCD3 relative to isotype, we observed enrichment
161 of pathways involved in chemokine production and chemokine receptor signaling, type I interferon
162 and antiviral responses, antigen processing and presentation, and phagocytosis/endocytosis
163 (Figure 2E). Thus, in this context, “microglial remodeling” reflects a coordinated re-balancing of

164 microglial programs: nasal aCD3 enhances transcriptional pathways that support immune
165 regulation, debris clearance, and maintenance of homeostasis in mice post-acute infection.
166 However, this early intervention window is unlikely to be practical for clinical implementation for
167 many individuals with Long COVID, who typically present months or even years after initial
168 infection (Bonilla et al., 2023).
169

170 **Delayed nasal aCD3 mAb induces brain Treg cells and reverses established**
171 **neuroinflammation in chronic post COVID setting**

172 To test whether nasal aCD3 can treat, rather than prevent, post-infectious CNS pathology, we
173 infected mice with SARS-CoV-2, allowed neuroinflammation to evolve for 4 weeks, and then
174 initiated nasal aCD3 or isotype control treatment (Figure 3A). Delayed nasal aCD3 administration
175 did not compromise antiviral immunity, as serum anti-spike IgG titers were comparable between
176 aCD3– and isotype-treated infected mice (Figure 3B). We next assessed whether late aCD3 could
177 still modify established gliosis. Quantitative immunostaining showed that IBA1+ microglia and
178 GFAP+ astrocytes remained elevated in subcortical white matter and hippocampus of isotype-
179 treated post-COVID mice, whereas aCD3 markedly reduced microglial and astrocytic cell
180 numbers across these regions, approaching mock levels (Figure 3C, 3D, S2A). Thus, nasal aCD3
181 mAb was able to attenuate chronic gliosis even when initiated weeks after infection.

182 Because Treg cells can restrain neuroinflammation through IL 10–dependent interactions with glia
183 (Ito et al., 2019; Liston et al., 2022), we asked whether therapeutic nasal aCD3 expands brain Treg
184 populations in post COVID setting as in other neuroinflammation mouse models (Izzy et al., 2025;
185 Mayo et al., 2016). Flow cytometric analysis of brain CD4+ T cells after one week of treatment
186 revealed that aCD3 significantly increased the frequency of Foxp3+ CD4+ T cells compared with
187 isotype-treated mild COVID mice (Figure 3E). Within this expanded Treg compartment, we

188 observed higher proportions of IL-10–producing Foxp3+ cells and latency associated peptide
189 (LAP)-expressing Foxp3+ cells, consistent with enrichment of functionally suppressive Treg
190 subsets (Figure 3E)(Gandhi et al., 2010; Rubtsov et al., 2008).
191 We previously linked elevated CCL11 to neuroinflammation in the mild COVID model and in
192 Long COVID patients with cognitive symptoms (Fernandez-Castaneda et al., 2022). Analysis of
193 cerebrospinal fluid showed that delayed nasal aCD3 shifted this cytokine–chemokine milieu
194 toward a more regulatory profile: IL-10 levels trended upward, while CCL11 concentrations were
195 significantly reduced relative to isotype-treated post-COVID mice (Figure 3F). Together, these
196 findings demonstrate that delayed nasal aCD3 remains effective when delivered after the acute
197 pulmonary phase, inducing IL-10–expressing brain Treg cells, normalizing CSF CCL11, and
198 dampening established microglial and astrocytic activation in mild COVID mice.
199

200 **Nasal anti-CD3 antibody treatment improves neurogenesis and cognitive function post-**
201 **COVID**

202 Because cognitive dysfunction is a common symptom of Long COVID (Hampshire et al., 2021),
203 we next asked whether nasal aCD3-mediated immune rebalancing improves downstream neural
204 outcomes by restoring hippocampal neurogenesis and memory performance. In line with prior
205 work (Fernandez-Castaneda et al., 2022), isotype-treated post-COVID mice showed a marked
206 reduction in Doublecortin (DCX)+ neuroblasts in the dentate gyrus compared with mock controls,
207 indicating impaired ongoing hippocampal neurogenesis. Nasal aCD3 significantly increased
208 DCX+ cell density in post-COVID mice, and this rescue was evident whether mAb was initiated
209 early (1 week after infection) or at a delayed time point (4 weeks after infection), indicating that
210 the treatment promotes hippocampal neurogenesis across a broad temporal window (Figure 4A).
211 To link these cellular changes to brain-wide cell states and behavior, we focused subsequent

212 experiments on the delayed treatment paradigm used for single-cell RNAseq and cognitive testing
213 (Figure 4B). For scRNA-seq, cerebrum tissue containing cortex, corpus callosum, and
214 hippocampus were dissociated from each group. We profiled 22,941 cells from isotype-treated
215 mild COVID mice, 24,395 cells from aCD3-treated mild COVID mice, and 13,458 cells from
216 mock controls and annotated 18 major cell populations based on canonical markers (Figure 4C,
217 S2B). At the level of broad classes, glial population frequencies were similar across conditions
218 (Figure S2C), whereas non-glial populations, particularly neuronal lineages, showed the largest
219 shifts with infection and treatment (Figure S2D). Stratifying by neuronal subtype revealed that
220 nasal aCD3 was associated with an expansion of immature neuron populations and a relative
221 reduction of mature excitatory neurons compared with isotype-treated post-COVID mice,
222 consistent with enhanced neuroblast production (Figure 4D).
223 Because microglia can undergo substantial state transitions without changing in abundance
224 (Fernandez-Castaneda et al., 2022), we next examined microglial transcriptional programs in the
225 single cell dataset. Intersection analysis of microglial DEGs across contrasts showed that most
226 transcriptional changes were specific to either infection (isotype vs mock) or treatment (aCD3 vs
227 isotype), with a smaller shared gene set regulated in both comparisons (Figure 4E). Microglia from
228 infected mice upregulated inflammatory and antigen presentation modules, whereas aCD3 induced
229 a partially overlapping but distinct program (Figure 4F). Notably, the inhibitory receptor Cd300lf
230 (Lu et al., 2024), which was elevated in microglia from isotype-treated mild COVID mice, was
231 reduced by aCD3, with the largest shift occurring within the homeostatic microglia cluster as
232 previously reported (Figure S2E, S2F)(Fernandez-Castaneda et al., 2022; Hammond et al., 2019),
233 suggesting restoration of a more surveillance-like state. Pathway enrichment of microglial genes
234 upregulated by aCD3 highlighted chemokine signaling/chemotaxis, phagosome and antigen-
235 processing modules, and regulatory signaling pathways including TGF-β–related terms, consistent

236 with enhanced immune regulation and debris clearance (Figure 4G). In contrast, genes
237 downregulated by aCD3 were enriched for leukocyte activation, NF-κB, and cytokine-mediated
238 inflammatory signaling pathways, indicating suppression of proinflammatory microglial programs
239 (Figure 4H).
240 We then tested whether these cellular and molecular changes coincided with improved cognition.
241 Using a modified novel object recognition test with a short time interval (5 min) to probe attention
242 and short term memory relevant to patient reported "brain fog"(Gibson et al., 2019), isotype-
243 treated mice at 8 weeks post infection failed to discriminate between familiar and novel objects
244 (Fig. 4I). In contrast, mild COVID mice treated with nasal aCD3 for 4 weeks showed a restored
245 preference for the novel object comparable to mock-infected animals, indicating rescue of attention
246 and short-term recognition memory (Figure 4I).
247 Given the Treg-biased mechanism of nasal aCD3, we asked whether circulating Treg programs are
248 linked to cognitive symptoms in people with Long COVID. Re-analysis of our MY-LC cohort
249 (Klein et al., 2023), which includes symptom surveys and PBMC profiling (Figure 4J), showed
250 that participants with Long COVID had neurological symptoms, including the cognitive
251 complaints like brain fog, dizziness, and memory problems, consistently exhibited reduced
252 circulating effTreg (Figure 4K) or nTreg (Figure 4L) compared with those without these symptoms.
253 Together, these data indicate that nasal aCD3 ameliorates persistent deficits in hippocampal
254 neurogenesis and short-term memory after mild respiratory SARS CoV-2 infection in mice, and
255 that reduced effector Treg levels in circulation are associated with cognitive symptoms reported
256 by patients with Long COVID, suggesting the role of Treg-mediated immune regulation in post-
257 acute infection cognitive dysfunction.
258

259 **Discussion:**

260 Persistent cognitive dysfunction after SARS CoV-2 infection is a major symptom in Long COVID,
261 and the biological circuits that remain amenable to intervention after symptoms are established are
262 only beginning to be defined (Iwasaki and Putrino, 2023; Peluso and Deeks, 2024). Converging
263 clinical and experimental data implicate neuroinflammation, including sustained microglial
264 reactivity, as a key mediator of the neurological manifestations of Long COVID (Fernandez-
265 Castaneda et al., 2022; Monje and Iwasaki, 2022). Here we show that nasal aCD3 mAb, delivered
266 either early after infection or during an established post-acute phase, induces IL 10–producing
267 Foxp3+ Treg cells, attenuates neuroinflammation, and restores hippocampal neurogenesis and
268 cognitive behavior in a mild, respiratory-restricted COVID model.

269

270 Multiple lines of evidence support a role for sustained microglial reactivity in neurological Long
271 COVID. Neuropathological and CSF studies have described microgliosis, astrogliosis, cytokine
272 elevation, and blood–brain barrier disruption in patients with persistent neurological symptoms,
273 including those who experienced only mild acute disease (Beiersdorfer et al., 2024; Farhadian et
274 al., 2023; Grant et al., 2024; Greene et al., 2024). Mild COVID mouse models converge on this
275 picture: mild, respiratory-restricted infection produces long-lasting microglial reactivity, myelin
276 damage, and impaired hippocampal neurogenesis in the absence of direct viral neuroinvasion
277 (Fernandez-Castaneda et al., 2022; Israelow et al., 2020). Microglia exhibited a consistent
278 transcriptional signature weeks after infection, with upregulation of antigen presentation,
279 interferon and NF-κB driven inflammatory pathways despite confinement of viral replication to
280 the lung(Grant et al., 2024). Nasal aCD3 reshaped this landscape when given either early or after
281 neuroinflammation was established, treatment reduced IBA1+ and GFAP+ cell densities in the
282 hippocampus and white matter. Normalization of receptors such as Cd300lf within homeostatic

283 microglia clusters (Fernandez-Castaneda et al., 2022; Keswani et al., 2020; Lu et al., 2024),
284 together with suppression of inflammatory modules and enhancement of phagosome and TGF β–
285 related pathways, is consistent with a shift from a chronically reactive, antigen-presenting state
286 toward a surveillance-like phenotype more compatible with circuit homeostasis and repair.
287
288 Treg cells provide a mechanistic bridge between mucosal aCD3 mAb and these neuroimmune
289 effects (Kuhn and Weiner, 2016). Tregs are central to restraining effector responses, enforcing
290 tolerance at barrier sites and sculpting tissue resident macrophage and microglial states (Dikiy and
291 Rudensky, 2023; Ito et al., 2019). Imbalanced Treg have been reported to be correlated with
292 COVID-19 severity and Long COVID (Galvan-Pena et al., 2021; Shahbaz et al., 2025). In our
293 model, nasal aCD3 expanded brain Foxp3+ CD4 T cells, including IL-10–producing and LAP
294 expressing subsets associated with potent suppressive function, without compromising established
295 antiviral humoral immunity as anti-spike antibody titer. This pattern argues that mucosal aCD3
296 does not broadly blunt antiviral immunity but instead skews T cell responses toward a regulatory
297 phenotype capable of entering the CNS (Ito et al., 2019; Liston et al., 2024). The association
298 between reduced circulating effector Tregs and cognitive symptom clusters in our Long COVID
299 cohort provides a translational mirror, alongside additional inflammatory biomarkers such as
300 CCL11 that have been linked to brain fog in prior studies (Fernandez-Castaneda et al., 2022;
301 Geraghty et al., 2025), suggesting that patients with regulatory deficits may be particularly benefit
302 from Treg- directed intervention.
303
304 At the neuronal level, nasal aCD3 rescued in hippocampal neurogenesis vulnerable to Long
305 COVID. Mild respiratory infection reduced DCX+ neuroblasts in the dentate gyrus and impaired
306 performance on a short delay novel object recognition task designed to probe aspects of “brain

307 fog," consistent with reports of long-lasting cognitive deficits and altered hippocampal structure
308 and connectivity in human cohorts (Zorzo et al., 2023). aCD3 restored dentate gyrus neurogenesis
309 across a broad temporal window and increased the representation of immature neuronal
310 populations while reducing mature excitatory neurons, consistent with enhanced ongoing dentate
311 neurogenesis and a shift in neuronal population balance (Disouky et al., 2026; Toni and Schinder,
312 2015). Prior work has implicated chemokines such as CCL11 as mediators of impaired
313 neurogenesis and white matter microglial activation in different chronic CNS inflammation models
314 (Fernandez-Castaneda et al., 2022; Geraghty et al., 2025; Villeda et al., 2011). In our delayed
315 treatment paradigm, nasal aCD3 increased IL-10 and reduced CCL11 in the CSF and IL-10
316 production from Tregs, identifying a Treg–IL-10–CCL11 axis as one route by which immune
317 rebalancing may release a brake on the neurogenic niche. Disentangling whether this axis acts
318 directly on neural progenitors or indirectly via microglia, astrocytes or the neurovascular unit will
319 require cell type specific manipulation of IL-10 and CCL11 signaling and longitudinal imaging of
320 neurogenesis and myelin integrity.
321
322 The nasal route offers practical and biological advantages for inducing this regulatory circuit (Wu
323 et al., 2008). The mucosal immune system is naturally biased toward tolerogenic responses, and
324 nasal aCD3 has been shown to expand IL 10–producing Tregs that home to the CNS and modulate
325 microglial activation in models of multiple sclerosis, Alzheimer's disease and traumatic brain
326 injury (Izzy et al., 2025; Lopes et al., 2023; Mayo et al., 2016). Foralumab, a fully human aCD3
327 formulated for nasal delivery, has been administered to people and produced immunomodulatory
328 effects with a favorable safety profile (Kuhn and Weiner, 2016; Singhal et al., 2025), including a
329 pilot trial in mild to moderate COVID 19 in which nasal foralumab reduced lung inflammation
330 and circulating inflammatory biomarkers without major adverse events (Moreira et al., 2023;

331 Moreira et al., 2021). Studies in progressive multiple sclerosis and have demonstrated nasal
332 foralumab dampens microglia reactivity as measured by TSPO-PET imaging, modulates the
333 immune system towards a regulatory phenotype and stabilizes disease(Chitnis et al., 2026; Tay et
334 al., 2026), further supporting the feasibility of nasal aCD3 as a CNS targeted immunotherapy. Our
335 findings here extend this concept to the post-acute phase of SARS CoV-2 infection, suggesting
336 that nasal aCD3 could provide a noninvasive means to modulate brain relevant immune circuits in
337 Long COVID.
338
339 Together, our findings identify nasal aCD3 as a candidate immunotherapy for Long COVID–
340 associated cognitive dysfunction that operates by inducing IL-10–competent Tregs,
341 reprogramming microglial states, normalizing chemokine milieus such as the CCL11 axis and
342 restoring hippocampal neurogenesis and a cognitive behavioral indicator of attention and short-
343 term memory. By integrating mechanistic mouse experiments with immune phenotyping in Long
344 COVID patients, this work supports a broader framework in which a subtype of Long COVID
345 with neuroimmune symptoms, characterized by effector Treg deficiency and persistent microglial
346 activation, could be targeted with biomarker-anchored interventions in post-viral
347 neuroinflammatory disease.
348
349 This study has several limitations. First, our mouse model was performed in female mice, a choice
350 motivated by reports of higher Long COVID symptom burden in women(Silva et al., 2024), but it
351 does not fully recapitulate the heterogeneous pathophysiology of human Long COVID. Second,
352 our mechanistic investigations identified the Treg-IL-10-CCL11 axis as a key mediator of
353 therapeutic benefit, but cell-type-specific loss-of-function studies will be required to definitively
354 establish whether this axis acts directly on neural progenitors or indirectly via microglia, astrocytes,

355 or the neurovascular unit. Third, cognitive assessment was limited to a single behavioral paradigm
356 (the modified novel object recognition test), which evaluated short-term recognition memory and
357 did not encompass other domains, such as executive function, and processing speed, because
358 behavioral studies were constrained by the requirements of BSL3 facility. Finally, our human
359 cohort analysis demonstrated associations between reduced circulating effector Tregs and
360 cognitive symptoms in Long COVID patients, but these data are observational and do not establish
361 causation. Despite these limitations, our findings provide a strong preclinical rationale to advance
362 nasal aCD3 mAb therapy toward clinical evaluation for Long COVID-associated cognitive
363 dysfunction.

364 **Methods:**

365 **Animal**

366 6- to 12-week-old female CD1 mice were purchased from Charles River and housed at Yale
367 University. Experiments with wild-type mice transduced with AAV-hACE2 were performed with
368 littermate controls. All procedures used in this study (sex and age matched) complied with federal
369 guidelines and the institutional policies of the Yale School of Medicine Animal Care and Use
370 Committee.

371 **Virus Stock**

372 As reported previously (Israelow et al., 2020), Vero E6 cells overexpressing angiotensin-
373 converting enzyme 2 (ACE2) and TMPRSS2 [kindly provided by B. Graham at the National
374 Institutes of Health Vaccine Research Center (NIH-VRC)] were infected with SARS-CoV-2 isolate
375 hCOV-19/USA-WA1/2020 (NR-52281; BEI Resources) at a M.O.I. of 0.01 for 2 days until
376 sufficient cytopathic effect was noted. After incubation, the supernatant was clarified by
377 centrifugation (5 min, 500g), filtered through a 0.45-µm filter. Virus containing supernatant was
378 applied to Amicon Ultra-15 centrifugal filter (Ultracel 100k) and spun at 2000 rpm for 15 minutes
379 prior to aliquoting and storage at -80°C. Viral titers were measured with a standard plaque assay
380 by using Vero E6 cells.

381 **AAV preparation**

382 Adeno-associated virus 9 encoding hACE2 (AAV-CMV-hACE2) were made through the Penn
383 vector core at University of Pennsylvania.

384 **AAV delivery and SARS-CoV2 infection**

385 To overexpress human ACE2 in the lower respiratory tract, CD1 mice were infected intratracheally
386 with AAV-hACE2 as previously described (Israelow et al., 2020). Briefly, animals were
387 anaesthetized using a mixture of ketamine (100 mg/kg) and xylazine (10 mg/kg), injected

388 intraperitoneally. The rostral neck was shaved and disinfected with iodine and ethanol. A 5-mm
389 incision was made, the salivary glands were retracted, and the trachea was visualized. Using a 500-
390 µl insulin syringe, a 50-µl bolus injection of 10^{11} genome copies (GC) of AAV- hACE2 was
391 injected into the trachea. The incision was closed with VetBond skin glue. After two weeks of
392 recovery, mice were anesthetized using 30% vol/vol isoflurane diluted in propylene glycol. Using
393 a pipette, 50 µl of SARS-CoV-2 (3×10^7 PFU/ml) was delivered intranasally

394 **Treatment with anti-CD3 mAb**

395 Mice were nasally treated with a daily antibody dose, starting either one week or four weeks after
396 SARS-CoV-2 infection for seven days. After one week of daily treatment, mice were treated with
397 the antibody every other day for an additional three weeks. Each mouse was given 1 µg of hamster
398 anti-mouse CD3 antibody (145-2C11, BioXCell) or hamster IgG control antibody (BioXCell)(Izzy
399 et al., 2025).

400 **Flowcytometry**

401 Brains were harvested from PBS perfusion mice and incubated in a digestion buffer containing 1
402 mg/ml collagenase D (Roche) and 16 µg/ml DNase I (Sigma-Aldrich) in HBSS at 37 °C for 30
403 min. Digested cell suspension was filtered through a 70-µm filter, followed by gradient
404 centrifugation enrichment with 30% Percoll. Enrihched brain cells were blocked with Fc blocker
405 (2.4G2, BioxCell) for 10 minutes on ice and then stained with aqua Live/Dead, Pacific blue anti-
406 mouse CD45 (30-F11, BioLegend), APC/cyanine7 anti-mouse CD11b (M1/70, BioLegend),
407 BV605 anti-mouse TCRβ (H57-597, BioLegend), APC anti-mouse CD4 (RM4-5, BioLegend) and
408 PE anti-mouse LAP (TW7-16B4, BioLegend) for 30 minutes on ice. Cells were washed to remove
409 excess antibodies and fixed with 4% PFA for 30 minutes before analysis. For intracellular staining,
410 surface-stained cells were fixed and permeabilized with the FOXP3/Transcription Factor Staining
411 Buffer Set (Thermo Fisher), followed by FITC anti-mouse Foxp3 staining (FJK-16s, Thermo

412 Fisher). Cells were washed and resuspended in PBS for analysis on an Attune NXT (Thermo
413 Fisher). Data were analyzed using FlowJo software version 10.8 software (BD)

414 **Cytokine/Chemokine screening**

415 The Luminex multiplex assay was performed by the Human Immune Monitoring Center at
416 Stanford University with Mouse 48-plex Procarta kits from Thermo Fisher as previously
417 described(Fernandez-Castaneda et al., 2022). CSF samples were measured as singlets, while serum
418 samples were measured in duplicate.

419 **Immunohistochemistry**

420 Mice were deeply anesthetized with isoflurane until respiration rate slowed and perfused
421 transcardially with Hank's Balanced Salt Solution (HBSS). Brains were isolated and fixed in 4%
422 paraformaldehyde (PFA) for 24-48 hours at 4°C. Following fixation, samples were sequentially
423 cryoprotected by incubation in 30% sucrose solution for 24 h. Brains were then embedded in
424 Tissue-Tek OCT compound (Sakura, compound 4583), snap-frozen, and preserved at -80 °C until
425 further processing. Brains were subsequently sectioned at -20 °C using a cryostat at the bregma
426 position for each targeted brain. Sections were cut in 0.2 mm in a sixfold series interval. Five total
427 sections were placed on Colorfrost Plus-treated adhesion slides (Thermo Fisher Scientific) and
428 stored at -20 °C until the time of staining. For immunofluorescent detection, sections were first
429 allowed to equilibrate to room temperature, then permeabilized and blocked for 1 hour in a 10%
430 normal horse serum solution, containing 0.1% Triton X-100, 1% glycine, and 2% bovine serum
431 albumin (BSA). Slides were incubated overnight at 4 °C with anti-Iba1 (rabbit, 1:500, Wako), DCX
432 (rabbit, 1:200, Abcam, cat.no. ab18723), or GFAP-AF488 conjugated antibody (mouse, 1:500,
433 Thermo fisher, cat.no. 53-9892-82). For unconjugated primary antibodies, the following day the
434 sections were washed and incubated with an Alexa Fluor-647 goat-anti rabbit IgG (1:1000, Thermo
435 Fisher, cat.no. A-21245) or Alexa Fluor-594 goat anti-rabbit IgG (1:1000, Thermo Fisher, cat.no.

436 A-11012). Stained slides were co-stained with DAPI mounting medium (Vector laboratories, cat.
437 no. UX-93952-24). Images were taken using an Olympus FV3000 series confocal laser scanning
438 microscope system on the 20x or 10x objective.

439 **Image analysis**

440 Quantification of Iba-1+, GFAP+, and DCX+ cells was performed using ImageJ
441 (https://imagej.nih.gov/ij). For each section, three representative photomicrographs were analyzed
442 (3-4 sections per animal), and cell counts were averaged per field of view. Regions of interest
443 (ROIs) were defined as 100 x 100 pixels, corresponding to a spatial resolution of 0.625 μm per
444 pixel. Numbers are represented as cells per mm2.

445 **Behavioral testing**

446 All behavioral assays were performed in a clean, empty rat cage (26.6 x 48.26 x 20.32 cm) covered
447 with white plastic wrap and placed in an ABSL3 level Biosafety Cabinet. Animals were handled
448 for 2 minutes for 4 days before subjecting to novel object recognition testing (NORT). One day
449 before the NORT, the mouse was placed in the center of the rat cage and allowed to habituate for
450 20 min. The NORT is a modified version with a shortened rest window between the training and
451 testing phase to evaluate the short-term memory (< 5 min) function. During the task, the mouse
452 was placed in the center of the cage to acclimate for 10 min before being returned to the home
453 cage for another 5 min. The mouse was then placed in the cage with two identical Lego objects for
454 5 min exploration and then returned to the home cage for 5 min. During this time, one object from
455 the training phase was replaced a new Lego object (of similar size, different shape and color) for
456 the testing phase. In the novel object testing phase, the mouse was returned to the cage and allowed
457 to explore for 10 min. The recorded video was analyzed using Noldus analysis software
458 (EthoVision XT 15). Only animals that explored both objects during the testing phase for an
459 accumulation of a minimum of 20s were included in the analysis.

460 **Sample preparation of Bulk RNAseq**

461 Mice were anesthetized with isoflurane and perfused intracardially with 10ml cold perfusion buffer.
462 Perfusion buffer, dissection buffer and digestion buffer were freshly prepared as previously
463 described(Marsh et al., 2022). Brains were quickly dissected and placed into an adult mouse brain
464 slicer matrix within dissection buffer. 3μm cerebrum slice was cut and contained cortex and corpus
465 callosum followed by chopping in digestion buffer. Chopped tissues were incubated for 45 minutes
466 at 37°C and triturated by pipetting every 15 minutes. After incubation, the cell suspension was
467 then passed through a 70μm filter. Cells were wash with completed DMEM and spun to pellet cells.
468 Cell pellets were resuspended in 40% Percoll and followed by spinning for 25 minutes at 650g.
469 The supernatant containing myelin debris was discarded and the pellet was resuspended in FACS
470 buffer (HBSS+1% FBS+1mM EDTA) with inhibitory cocktail (Actinomycin
471 D+Triptolide+Anisomycin).

472 For FACS sorting, the cells were resuspended in FC blocker solution (2.4G2, BioxCell) and
473 incubated on ice for 10 mins. Cocktails of desired staining antibodies including live-dead Aqua,
474 PE-anti-CD11b (M1/70, BioLegend) and Alexafluor647 anti-CD45 (30-F11, BioLegend) were
475 added directly to cell suspension for 20 minutes incubation at 4°C. Prior to sort, cell were washed
476 and resuspend with FACS buffer. Stained cells were sorted by BD FACSAria (BD Biosciences).
477 RNA were extracted from sorted cells via the Qiagen Kit and submitted to Yale Center for Genome
478 Analysis, who then created cDNA libraries and sequenced on IlluminaSeq at 100 million reads per
479 sample.

480 All procedures except RNA extraction and sequencing were processed in Yale BSL-3 facility.

481 **Sample preparation and data analysis of scRNAseq**

482 Single cell suspension were prepared as the samples for bulk RNAseq and loaded onto the
483 Chromium Controller (10x Genomics) for droplet formation. scRNA-seq libraries were prepared

484 using the Chromium Single Cell 3'Reagent Kit (10x Genomics), according to manufacturer's
485 protocol. Samples were sequenced on the NovaSeq 6000 with 28-bp read 1, 8-bp i7 index and 98-
486 bp read 2 for the gene-expression library. Sequencing results were demultiplexed into Fastq files
487 using the Cell Ranger (10x Genomics, 6.1.2) mkfastq function. Samples were aligned to mm10-
488 2.2.0 10x genome. All procedures except sequencing were processed in Yale BSL-3 facility.

489 **Bioinformatics analysis**

490 *Mapping of bulk RNA-seq libraries and differential gene expression analysis*

491 Initially raw reads served as input for Trimmomatic 0.40 (Bolger et al., 2014), which performed
492 quality filtering removing Illumina adaptor sequences, low quality bases (phred score quality >
493 20), and short reads (PE -phred33 ILLUMINACLIP:truseq.fa:2:30:10 LEADING:3 TRAILING:3
494 SLIDINGWINDOW:3:20 MINLEN:36). Trimming was followed by rRNA filtering by
495 SortMeRNA software (Kopylova et al., 2012) using the SILVA rRNA library (Yilmaz et al., 2014)
496 as reference. Next the reads were mapped against the Genome Reference Consortium Mouse Build
497 39 (GRCm39) and the transcript abundance was quantified using Salmon v1.10.2 (Patro et al.,
498 2017). Finally, the count data were direct to differential analysis with DESeq2 (version 1.48.1) R
499 4.5 package (Love et al., 2014). The Cook's distance together with Principal components analysis
500 and hierarchical clustering of the 1000 most variable genes were used to identify outliers.

501 *Mouse brain scRNA-seq analysis*

502 Reads were aligned to the mouse genome (refdata-gex-mm10-2020-A) using Cell Ranger software
503 (v.7.0.1) (10x Genomics) generating the raw gene counts matrix. These count matrixes served as
504 input to downstream analysis in Seurat (version 5.1.0) (Hao et al., 2021), initially filtering cells
505 with unique molecular identifiers over 5,000 or less than 500, besides outliers with more than 5%
506 mitochondrial counts. The feature expression measurements for each cell were normalized by the
507 total expression, multiplied by the scale factor (10,000), and log transformed. We calculated the

508 3,000 highly variable genes to be used as integration anchors as we merged the three cohorts,
509 followed by linear transformation (scaling) regressing out heterogeneity associated with
510 mitochondrial contamination and UMI counts. Linear dimensional reduction was performed by
511 PCA, followed by non-linear UMAP embedding using the first 30 principal components, same
512 parameter used for clustering with FindNeighbors and FindClusters (0.9 resolution) Seurat's
513 functions. Differential gene-expression comparison between groups was done based on the non-
514 parametric Wilcoxon rank sum test. Genes with fold change > 1.5 (absolute value), adjusted P
515 value (Bonferroni correction) < 0.1 and detected in a minimum fraction of 20% cells in either of
516 the two populations were considered differentially expressed.

517 *Pathway analysis*

518 Biological process and Gene Ontology terms search and analysis were performed through online
519 database PANTHER 19.0 (Mi et al., 2019), Enrichr-KG (Chen et al., 2013; Kuleshov et al., 2016;
520 Xie et al., 2021), Metascape (Zhou et al., 2019) and WebGestalt (Elizarraras et al., 2024) with
521 standard parameters.

522 **Data and code availability**

523 The bulk RNAseq and scRNAseq raw data presented in this work will be publicly available at the
524 Sequence Read Archive (SRA) after publication. Bulk and scRNA-seq data is submitted to SRA.
525 with the following accession codes.

526 **<u>Acknowledgements:</u>**

527 The authors would like to thank members of the Yale Center for Genomic Analysis (YCGA) and
528 the Rodent Behavior Analysis facility at Yale Kavli Institute for Neuroscience. This study was
529 funded by National Institutes of Health (K08NS123503 to S.I.), Stepping Strong Breakthrough
530 Award from Gillian Reny Stepping Strong Center for Trauma Innovation (to S.I.), Department of
531 Defense (HT9425-24-1-0635, W911NF-23-1-0276, and SC240188 to S.I.), the Howard Hughes

532 Medical Institute Emerging Pathogens Initiative (to M.M. and A.I.), the Howard Hughes Medical
533 Institute (to M.M. and A.I.), and the Else Kröner Fresenius Prize for Medical Research 2023 (to
534 A.I.).

535

536 **Author Contributions:**

537 P.L., S.I., A.I. and H.L.W. planned the project; P.L. and S.I. designed, analyzed and interpreted
538 data and wrote the manuscript; P.L., S.I., T.Y., H.T.I., J.R.C., P.D.S., M.H.A.M., A.A. performed
539 experiments and analyzed data; review and editing by P.L., S.I., T.Y., H.T.I., J.R.C., P.D.S.,
540 M.H.A.M., A.A., T.G.M., M.M., A.I. and H.L.W.; supervised by S.I., A.I. and H.L.W.; funding
541 acquisition by S.I., M. M, A.I. and H.L.W..

542 **Declaration of Conflict of Interest:**

543 H.L.W. is on the scientific advisory board of Tiziana Life Sciences. A.I. co-founded RIGImmune,
544 Rho Bio., Xanadu Bio, PanV, and is a member of the Board of Directors of Roche Holding Ltd
545 and Genentech. All other authors declare no conflict of interest.

546

547 **References:**

548 Al-Aly, Z., Davis, H., McCorkell, L., Soares, L., Wulf-Hanson, S., Iwasaki, A., and Topol, E.J. (2024).
549 Long COVID science, research and policy. Nat Med *30*, 2148-2164.
550 Beiersdorfer, A., Rotermund, N., Schulz, K., Busch, M., Hirnet, D., Henne, S., Schwarzenberg, F.L.,
551 Dottermusch, M., Ondruschka, B., Matschke, J.*, et al.* (2024). Microgliosis, astrogliosis and loss
552 of aquaporin-4 polarity in frontal cortex of COVID-19 patients. bioRxiv.
553 Bolger, A.M., Lohse, M., and Usadel, B. (2014). Trimmomatic: a flexible trimmer for Illumina
554 sequence data. Bioinformatics *30*, 2114-2120.
555 Bonhenry, D., Charnley, M., Goncalves, J., Hammarstrom, P., Heneka, M.T., Itzhaki, R., Lambert,
556 J.C., Mannan, M., Baig, A.M., Middeldorp, J.*, et al.* (2024). SARS-CoV-2 infection as a cause of
557 neurodegeneration. Lancet Neurol *23*, 562-563.
558 Bonilla, H., Peluso, M.J., Rodgers, K., Aberg, J.A., Patterson, T.F., Tamburro, R., Baizer, L.,
559 Goldman, J.D., Rouphael, N., Deitchman, A.*, et al.* (2023). Therapeutic trials for long COVID-19:
560 A call to action from the interventions taskforce of the RECOVER initiative. Front Immunol *14*,
561 1129459.
562 Braga, J., Lepra, M., Kish, S.J., Rusjan, P.M., Nasser, Z., Verhoeff, N., Vasdev, N., Bagby, M.,
563 Boileau, I., Husain, M.I.*, et al.* (2023). Neuroinflammation After COVID-19 With Persistent
564 Depressive and Cognitive Symptoms. JAMA Psychiatry *80*, 787-795.
565 Bruno, R.M., Badhwar, S., Abid, L., Agharazii, M., Anastasio, F., Bellien, J., Burghuber, O., Faconti,
566 L., Filipovsky, J., Ghiadoni, L.*, et al.* (2025). Accelerated vascular ageing after COVID-19 infection:
567 the CARTESIAN study. Eur Heart J *46*, 3905-3918.
568 Chatenoud, L., and Bluestone, J.A. (2007). CD3-specific antibodies: a portal to the treatment of
569 autoimmunity. Nat Rev Immunol *7*, 622-632.
570 Chen, E.Y., Tan, C.M., Kou, Y., Duan, Q., Wang, Z., Meirelles, G.V., Clark, N.R., and Ma'ayan, A.
571 (2013). Enrichr: interactive and collaborative HTML5 gene list enrichment analysis tool. BMC
572 Bioinformatics *14*, 128.
573 Chitnis, T., Singhal, T., Zurawski, J., Saraceno, T.J., Gopalakrishnan, N., Cain, L., LaBarre, B., King,
574 D., Bergmark, R.W., Maxfield, A.Z.*, et al.* (2026). Nasal Foralumab for the Treatment of
575 Progression Independent of Relapses in Patients With Nonactive Secondary Progressive Multiple
576 Sclerosis. Neurology Neuroimmunology & Neuroinflammation *13*, e200543.
577 Davis, H.E., McCorkell, L., Vogel, J.M., and Topol, E.J. (2023). Long COVID: major findings,
578 mechanisms and recommendations. Nat Rev Microbiol *21*, 133-146.
579 Dikiy, S., and Rudensky, A.Y. (2023). Principles of regulatory T cell function. Immunity *56*, 240-
580 255.
581 Disouky, A., Sanborn, M.A., Sabitha, K.R., Mostafa, M.M., Ayala, I.A., Bennett, D.A., Lu, Y., Zhou,

582 Y., Keene, C.D., Weintraub, S.*, et al.* (2026). Human hippocampal neurogenesis in adulthood,
583 ageing and Alzheimer's disease. Nature.
584 Elizarraras, J.M., Liao, Y., Shi, Z., Zhu, Q., Pico, A.R., and Zhang, B. (2024). WebGestalt 2024:
585 faster gene set analysis and new support for metabolomics and multi-omics. Nucleic Acids Res
586 *52*, W415-W421.
587 Ellen, A. (2025). From Stagnation to Strategy: Challenges in Advancing Long COVID Research. J
588 Eval Clin Pract *31*, e70180.
589 Eng, L.F., Vanderhaeghen, J.J., Bignami, A., and Gerstl, B. (1971). An acidic protein isolated from
590 fibrous astrocytes. Brain Res *28*, 351-354.
591 Farhadian, S.F., Reisert, H.D., McAlpine, L., Chiarella, J., Kosana, P., Yoon, J., and Spudich, S.
592 (2023). Self-Reported Neuropsychiatric Post-COVID-19 Condition and CSF Markers of
593 Neuroinflammation. JAMA Netw Open *6*, e2342741.
594 Fernandez-Castaneda, A., Lu, P., Geraghty, A.C., Song, E., Lee, M.H., Wood, J., O'Dea, M.R.,
595 Dutton, S., Shamardani, K., Nwangwu, K.*, et al.* (2022). Mild respiratory COVID can cause multi-
596 lineage neural cell and myelin dysregulation. Cell *185*, 2452-2468 e2416.
597 Fujimoto, Y., Abe, H., Eiro, T., Tsugawa, S., Tanaka, M., Hatano, M., Nakajima, W., Ichijo, S.,
598 Arisawa, T., Takada, Y.*, et al.* (2025). Systemic increase of AMPA receptors associated with
599 cognitive impairment of long COVID. Brain Commun *7*, fcaf337.
600 Galvan-Pena, S., Leon, J., Chowdhary, K., Michelson, D.A., Vijaykumar, B., Yang, L., Magnuson,
601 A.M., Chen, F., Manickas-Hill, Z., Piechocka-Trocha, A.*, et al.* (2021). Profound Treg perturbations
602 correlate with COVID-19 severity. Proc Natl Acad Sci U S A *118*.
603 Gandhi, R., Farez, M.F., Wang, Y., Kozoriz, D., Quintana, F.J., and Weiner, H.L. (2010). Cutting
604 edge: human latency-associated peptide+ T cells: a novel regulatory T cell subset. J Immunol
605 *184*, 4620-4624.
606 Geraghty, A.C., Acosta-Alvarez, L., Rotiroti, M.C., Dutton, S., O'Dea, M.R., Kim, W., Trivedi, V.,
607 Mancusi, R., Shamardani, K., Malacon, K.*, et al.* (2025). Immunotherapy-related cognitive
608 impairment after CAR T cell therapy in mice. Cell *188*, 3238-3258 e3225.
609 Gibson, E.M., Nagaraja, S., Ocampo, A., Tam, L.T., Wood, L.S., Pallegar, P.N., Greene, J.J.,
610 Geraghty, A.C., Goldstein, A.K., Ni, L.*, et al.* (2019). Methotrexate Chemotherapy Induces
611 Persistent Tri-glial Dysregulation that Underlies Chemotherapy-Related Cognitive Impairment.
612 Cell *176*, 43-55 e13.
613 Grant, R.A., Poor, T.A., Sichizya, L., Diaz, E., Bailey, J.I., Soni, S., Senkow, K.J., Perez-Leonor, X.G.,
614 Abdala-Valencia, H., Lu, Z.*, et al.* (2024). Prolonged exposure to lung-derived cytokines is
615 associated with activation of microglia in patients with COVID-19. JCI Insight *9*.
616 Green, R., Marjenberg, Z., Lip, G.Y.H., Banerjee, A., Wisnivesky, J., Delaney, B.C., Peluso, M.J.,
617 Wynberg, E., and Abduljawad, S. (2025). A systematic review and meta-analysis of the impact of

618 vaccination on prevention of long COVID. Nat Commun *16*, 10326.
619 Greene, C., Connolly, R., Brennan, D., Laffan, A., O'Keeffe, E., Zaporojan, L., O'Callaghan, J.,
620 Thomson, B., Connolly, E., Argue, R.*, et al.* (2024). Blood-brain barrier disruption and sustained
621 systemic inflammation in individuals with long COVID-associated cognitive impairment. Nat
622 Neurosci *27*, 421-432.
623 Groff, D., Sun, A., Ssentongo, A.E., Ba, D.M., Parsons, N., Poudel, G.R., Lekoubou, A., Oh, J.S.,
624 Ericson, J.E., Ssentongo, P.*, et al.* (2021). Short-term and Long-term Rates of Postacute Sequelae
625 of SARS-CoV-2 Infection: A Systematic Review. JAMA Netw Open *4*, e2128568.
626 Hamlin, R.E., and Blish, C.A. (2024). Challenges and opportunities in long COVID research.
627 Immunity *57*, 1195-1214.
628 Hammond, T.R., Dufort, C., Dissing-Olesen, L., Giera, S., Young, A., Wysoker, A., Walker, A.J.,
629 Gergits, F., Segel, M., Nemesh, J.*, et al.* (2019). Single-Cell RNA Sequencing of Microglia
630 throughout the Mouse Lifespan and in the Injured Brain Reveals Complex Cell-State Changes.
631 Immunity *50*, 253-271 e256.
632 Hampshire, A., Trender, W., Chamberlain, S.R., Jolly, A.E., Grant, J.E., Patrick, F., Mazibuko, N.,
633 Williams, S.C., Barnby, J.M., Hellyer, P.*, et al.* (2021). Cognitive deficits in people who have
634 recovered from COVID-19. EClinicalMedicine *39*, 101044.
635 Hao, Y., Hao, S., Andersen-Nissen, E., Mauck, W.M., 3rd, Zheng, S., Butler, A., Lee, M.J., Wilk,
636 A.J., Darby, C., Zager, M.*, et al.* (2021). Integrated analysis of multimodal single-cell data. Cell
637 *184*, 3573-3587 e3529.
638 Hol, E.M., and Pekny, M. (2015). Glial fibrillary acidic protein (GFAP) and the astrocyte
639 intermediate filament system in diseases of the central nervous system. Curr Opin Cell Biol *32*,
640 121-130.
641 Israelow, B., Song, E., Mao, T., Lu, P., Meir, A., Liu, F., Alfajaro, M.M., Wei, J., Dong, H., Homer,
642 R.J.*, et al.* (2020). Mouse model of SARS-CoV-2 reveals inflammatory role of type I interferon
643 signaling. J Exp Med *217*.
644 Ito, M., Komai, K., Mise-Omata, S., Iizuka-Koga, M., Noguchi, Y., Kondo, T., Sakai, R., Matsuo, K.,
645 Nakayama, T., Yoshie, O.*, et al.* (2019). Brain regulatory T cells suppress astrogliosis and
646 potentiate neurological recovery. Nature *565*, 246-250.
647 Iwasaki, A., and Putrino, D. (2023). Why we need a deeper understanding of the
648 pathophysiology of long COVID. Lancet Infect Dis *23*, 393-395.
649 Izzy, S., Yahya, T., Albastaki, O., Abou-El-Hassan, H., Aronchik, M., Cao, T., De Oliveira, M.G., Lu,
650 K.J., Moreira, T.G., da Silva, P.*, et al.* (2025). Nasal anti-CD3 monoclonal antibody ameliorates
651 traumatic brain injury, enhances microglial phagocytosis and reduces neuroinflammation via IL-
652 10-dependent T(reg)-microglia crosstalk. Nat Neurosci *28*, 499-516.
653 Jansen, E.B., Orvold, S.N., Swan, C.L., Yourkowski, A., Thivierge, B.M., Francis, M.E., Ge, A.,

654 Rioux, M., Darbellay, J., Howland, J.G.*, et al.* (2022). After the virus has cleared-Can preclinical
655 models be employed for Long COVID research? PLoS Pathog *18*, e1010741.
656 Keswani, T., Roland, J., Herbert, F., Delcroix-Genete, D., Bauderlique-Le Roy, H., Gaayeb, L.,
657 Cazenave, P.A., and Pied, S. (2020). Expression of CD300lf by microglia contributes to resistance
658 to cerebral malaria by impeding the neuroinflammation. Genes Immun *21*, 45-62.
659 Klein, J., Wood, J., Jaycox, J.R., Dhodapkar, R.M., Lu, P., Gehlhausen, J.R., Tabachnikova, A.,
660 Greene, K., Tabacof, L., Malik, A.A.*, et al.* (2023). Distinguishing features of long COVID identified
661 through immune profiling. Nature *623*, 139-148.
662 Kopylova, E., Noe, L., and Touzet, H. (2012). SortMeRNA: fast and accurate filtering of ribosomal
663 RNAs in metatranscriptomic data. Bioinformatics *28*, 3211-3217.
664 Kuhn, C., and Weiner, H.L. (2016). Therapeutic anti-CD3 monoclonal antibodies: from bench to
665 bedside. Immunotherapy *8*, 889-906.
666 Kuleshov, M.V., Jones, M.R., Rouillard, A.D., Fernandez, N.F., Duan, Q., Wang, Z., Koplev, S.,
667 Jenkins, S.L., Jagodnik, K.M., Lachmann, A.*, et al.* (2016). Enrichr: a comprehensive gene set
668 enrichment analysis web server 2016 update. Nucleic Acids Res *44*, W90-97.
669 Liston, A., Dooley, J., and Yshii, L. (2022). Brain-resident regulatory T cells and their role in health
670 and disease. Immunol Lett *248*, 26-30.
671 Liston, A., Pasciuto, E., Fitzgerald, D.C., and Yshii, L. (2024). Brain regulatory T cells. Nat Rev
672 Immunol *24*, 326-337.
673 Lopes, J.R., Zhang, X., Mayrink, J., Tatematsu, B.K., Guo, L., LeServe, D.S., Abou-El-Hassan, H.,
674 Rong, F., Dalton, M.J., Oliveira, M.G.*, et al.* (2023). Nasal administration of anti-CD3 monoclonal
675 antibody ameliorates disease in a mouse model of Alzheimer's disease. Proc Natl Acad Sci U S A
676 *120*, e2309221120.
677 Love, M.I., Huber, W., and Anders, S. (2014). Moderated estimation of fold change and
678 dispersion for RNA-seq data with DESeq2. Genome Biol *15*, 550.
679 Lu, Z., Liu, Z., Wang, C., Jiang, R., Wang, Z., Liao, W., Wang, W., Chen, J., Zhu, X., Zhao, J.*, et al.*
680 (2024). CD300LF(+) microglia impede the neuroinflammation following traumatic brain injury by
681 inhibiting STING pathway. CNS Neurosci Ther *30*, e14824.
682 Marsh, S.E., Walker, A.J., Kamath, T., Dissing-Olesen, L., Hammond, T.R., de Soysa, T.Y., Young,
683 A.M.H., Murphy, S., Abdulraouf, A., Nadaf, N.*, et al.* (2022). Dissection of artifactual and
684 confounding glial signatures by single-cell sequencing of mouse and human brain. Nat Neurosci
685 *25*, 306-316.
686 Mayo, L., Cunha, A.P., Madi, A., Beynon, V., Yang, Z., Alvarez, J.I., Prat, A., Sobel, R.A., Kobzik, L.,
687 Lassmann, H.*, et al.* (2016). IL-10-dependent Tr1 cells attenuate astrocyte activation and
688 ameliorate chronic central nervous system inflammation. Brain *139*, 1939-1957.
689 Mi, H., Muruganujan, A., Huang, X., Ebert, D., Mills, C., Guo, X., and Thomas, P.D. (2019).

690 Protocol Update for large-scale genome and gene function analysis with the PANTHER
691 classification system (v.14.0). Nat Protoc *14*, 703-721.
692 Monje, M., and Iwasaki, A. (2022). The neurobiology of long COVID. Neuron *110*, 3484-3496.
693 Moreira, T., Gauthier, C.D., Murphy, L., Lanser, T.B., Paul, A., Matos, K.T.F., Mangani, D., Izzy, S.,
694 Rezende, R.M., Healy, B.C.*, et al.* (2023). Nasal administration of anti-CD3 mAb (Foralumab)
695 downregulates NKG7 and increases TGFB1 and GIMAP7 expression in T cells in subjects with
696 COVID-19. Proc Natl Acad Sci U S A *120*, e2220272120.
697 Moreira, T.G., Matos, K.T.F., De Paula, G.S., Santana, T.M.M., Da Mata, R.G., Pansera, F.C.,
698 Cortina, A.S., Spinola, M.G., Baecher-Allan, C.M., Keppeke, G.D.*, et al.* (2021). Nasal
699 Administration of Anti-CD3 Monoclonal Antibody (Foralumab) Reduces Lung Inflammation and
700 Blood Inflammatory Biomarkers in Mild to Moderate COVID-19 Patients: A Pilot Study. Front
701 Immunol *12*, 709861.
702 Mukherjee, S., Singer, T., Venkatesh, A., Choudhury, N.A., Perez Giraldo, G.S., Jimenez, M.,
703 Miller, J., Lopez, M., Hanson, B.A., Bawa, A.P.*, et al.* (2025). Vaccination prior to SARS-CoV-2
704 infection does not affect the neurologic manifestations of long COVID. Brain Commun *7*,
705 fcae448.
706 Nalbandian, A., Sehgal, K., Gupta, A., Madhavan, M.V., McGroder, C., Stevens, J.S., Cook, J.R.,
707 Nordvig, A.S., Shalev, D., Sehrawat, T.S.*, et al.* (2021). Post-acute COVID-19 syndrome. Nat Med
708 *27*, 601-615.
709 Notarte, K.I., Catahay, J.A., Velasco, J.V., Pastrana, A., Ver, A.T., Pangilinan, F.C., Peligro, P.J.,
710 Casimiro, M., Guerrero, J.J., Gellaco, M.M.L.*, et al.* (2022). Impact of COVID-19 vaccination on
711 the risk of developing long-COVID and on existing long-COVID symptoms: A systematic review.
712 EClinicalMedicine *53*, 101624.
713 Ochi, H., Abraham, M., Ishikawa, H., Frenkel, D., Yang, K., Basso, A.S., Wu, H., Chen, M.L.,
714 Gandhi, R., Miller, A.*, et al.* (2006). Oral CD3-specific antibody suppresses autoimmune
715 encephalomyelitis by inducing CD4+ CD25- LAP+ T cells. Nat Med *12*, 627-635.
716 Pagliano, P., Salzano, F., D'Amore, C., Spera, A., Conti, V., Folliero, V., Franci, G., and Ascione, T.
717 (2025). How do drug discovery scientists address the unmet need of long COVID syndrome
718 therapeutics and what more can be done? Expert Opin Drug Discov *20*, 1251-1265.
719 Patro, R., Duggal, G., Love, M.I., Irizarry, R.A., and Kingsford, C. (2017). Salmon provides fast and
720 bias-aware quantification of transcript expression. Nat Methods *14*, 417-419.
721 Peluso, M.J., and Deeks, S.G. (2024). Mechanisms of long COVID and the path toward
722 therapeutics. Cell *187*, 5500-5529.
723 Rubtsov, Y.P., Rasmussen, J.P., Chi, E.Y., Fontenot, J., Castelli, L., Ye, X., Treuting, P., Siewe, L.,
724 Roers, A., Henderson, W.R., Jr.*, et al.* (2008). Regulatory T cell-derived interleukin-10 limits
725 inflammation at environmental interfaces. Immunity *28*, 546-558.

726 Saikarthik, J., Saraswathi, I., Padhi, B.K., Shamim, M.A., Alzerwi, N., Alarifi, A., and Gandhi, A.P.
727 (2025). Structural and functional neuroimaging of hippocampus to study adult neurogenesis in
728 long COVID-19 patients with neuropsychiatric symptoms: a scoping review. PeerJ *13*, e19575.
729 Seo, D., Choi, Y., Jeong, E., Bang, S., Lee, J.S., Jang, I.H., Choi, L., Kim, J.H., Shin, W., Seo, B.R.*, et*
730 *al.* (2025). Distinct brain alterations and neurodegenerative processes in cognitive impairment
731 associated with post-acute sequelae of COVID-19. Nat Commun *16*, 10552.
732 Shahbaz, S., Osman, M., Syed, H., Mason, A., Rosychuk, R.J., Cohen Tervaert, J.W., and Elahi, S.
733 (2025). Integrated immune, hormonal, and transcriptomic profiling reveals sex-specific
734 dysregulation in long COVID patients with ME/CFS. Cell Rep Med *6*, 102449.
735 Silva, J., Takahashi, T., Wood, J., Lu, P., Tabachnikova, A., Gehlhausen, J.R., Greene, K.,
736 Bhattacharjee, B., Monteiro, V.S., Lucas, C.*, et al.* (2024). Sex differences in symptomatology and
737 immune profiles of Long COVID. medRxiv.
738 Singhal, T., Cicero, S., Gale, S.A., Horan, N., Dubey, S., Marshall, G.A., and Weiner, H.L. (2025).
739 Dampening of Microglial Activation With Nasal Foralumab Administration in Moderate
740 Alzheimer's Disease Dementia. Clin Nucl Med *50*, 756-757.
741 Tay, D., Ahmed, H., Dawoud, A., Salam, M., Gobbi, L., Grether, U., Edelmann, M.R., Wittwer,
742 M.B., Collin, L., Atz, K.*, et al.* (2026). Translational molecular imaging and drug development in
743 multiple sclerosis. Theranostics *16*, 1630-1657.
744 Toni, N., and Schinder, A.F. (2015). Maturation and Functional Integration of New Granule Cells
745 into the Adult Hippocampus. Cold Spring Harb Perspect Biol *8*, a018903.
746 Vanderheiden, A., Hill, J.D., Jiang, X., Deppen, B., Bamunuarachchi, G., Soudani, N., Joshi, A.,
747 Cain, M.D., Boon, A.C.M., and Klein, R.S. (2024). Vaccination reduces central nervous system IL-
748 1beta and memory deficits after COVID-19 in mice. Nat Immunol *25*, 1158-1171.
749 Vignali, D.A., Collison, L.W., and Workman, C.J. (2008). How regulatory T cells work. Nat Rev
750 Immunol *8*, 523-532.
751 Villeda, S.A., Luo, J., Mosher, K.I., Zou, B., Britschgi, M., Bieri, G., Stan, T.M., Fainberg, N., Ding,
752 Z., Eggel, A.*, et al.* (2011). The ageing systemic milieu negatively regulates neurogenesis and
753 cognitive function. Nature *477*, 90-94.
754 Weiner, H.L., da Cunha, A.P., Quintana, F., and Wu, H. (2011). Oral tolerance. Immunol Rev *241*,
755 241-259.
756 Wu, H.Y., Quintana, F.J., and Weiner, H.L. (2008). Nasal anti-CD3 antibody ameliorates lupus by
757 inducing an IL-10-secreting CD4+ CD25- LAP+ regulatory T cell and is associated with down-
758 regulation of IL-17+ CD4+ ICOS+ CXCR5+ follicular helper T cells. J Immunol *181*, 6038-6050.
759 Xie, Z., Bailey, A., Kuleshov, M.V., Clarke, D.J.B., Evangelista, J.E., Jenkins, S.L., Lachmann, A.,
760 Wojciechowicz, M.L., Kropiwnicki, E., Jagodnik, K.M.*, et al.* (2021). Gene Set Knowledge
761 Discovery with Enrichr. Curr Protoc *1*, e90.

762 Xu, E., Xie, Y., and Al-Aly, Z. (2022). Long-term neurologic outcomes of COVID-19. Nat Med *28*,
763 2406-2415.
764 Yilmaz, P., Parfrey, L.W., Yarza, P., Gerken, J., Pruesse, E., Quast, C., Schweer, T., Peplies, J.,
765 Ludwig, W., and Glockner, F.O. (2014). The SILVA and "All-species Living Tree Project (LTP)"
766 taxonomic frameworks. Nucleic Acids Res *42*, D643-648.
767 Yin, K., Peluso, M.J., Luo, X., Thomas, R., Shin, M.G., Neidleman, J., Andrew, A., Young, K.C., Ma,
768 T., Hoh, R.*, et al.* (2024). Long COVID manifests with T cell dysregulation, inflammation and an
769 uncoordinated adaptive immune response to SARS-CoV-2. Nat Immunol *25*, 218-225.
770 Zhou, Y., Zhou, B., Pache, L., Chang, M., Khodabakhshi, A.H., Tanaseichuk, O., Benner, C., and
771 Chanda, S.K. (2019). Metascape provides a biologist-oriented resource for the analysis of
772 systems-level datasets. Nat Commun *10*, 1523.
773 Zorzo, C., Solares, L., Mendez, M., and Mendez-Lopez, M. (2023). Hippocampal alterations after
774 SARS-CoV-2 infection: A systematic review. Behav Brain Res *455*, 114662.
775
776

Figure 1

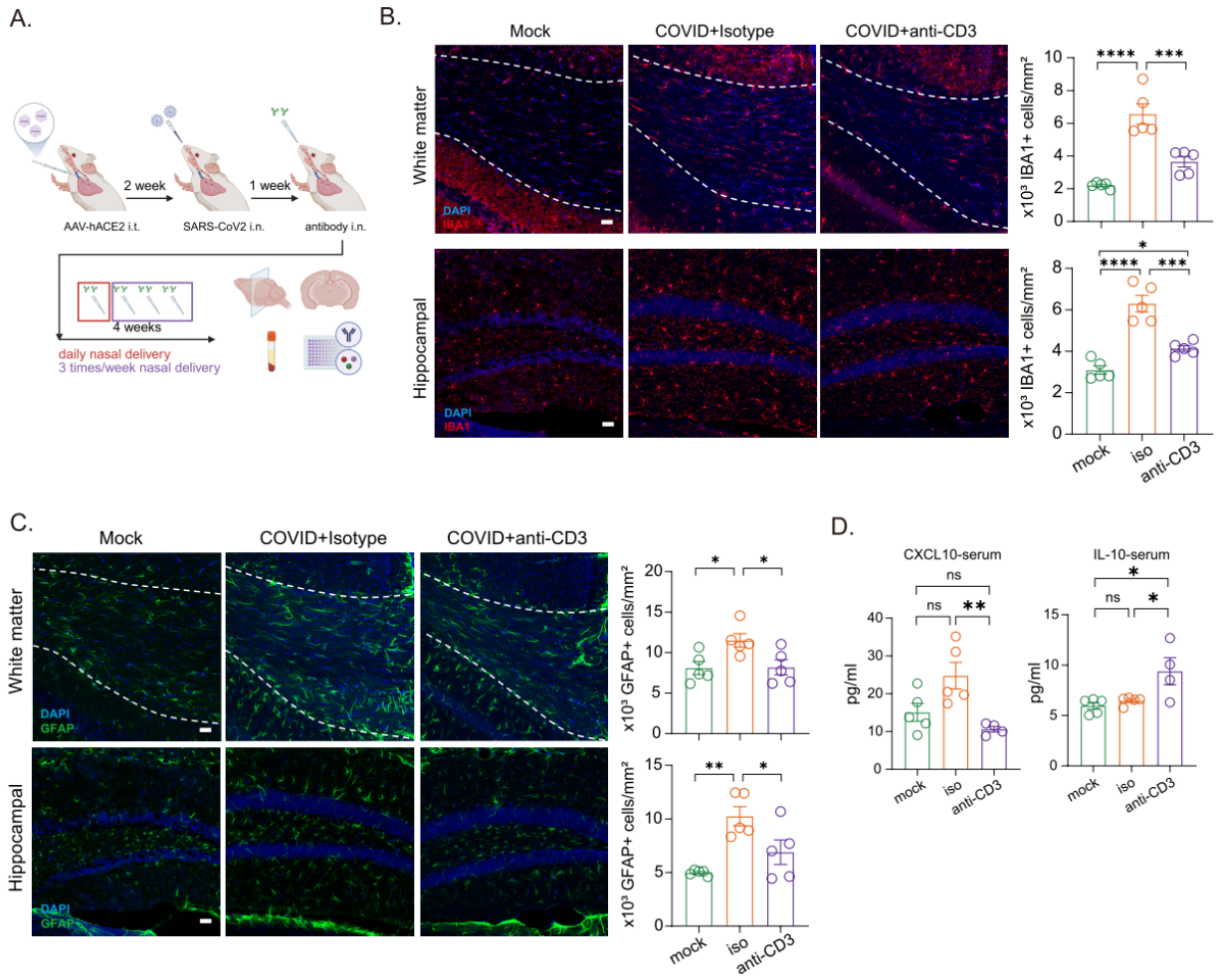

Figure. 1 Nasal anti-CD3 treatment reduces CNS neuroinflammation after acute SARS CoV-2 infection. (A) Experimental paradigm for intranasal anti-CD3 administration in the mild COVID mouse model. Mice expressing human ACE2 received respiratory restricted SARS CoV-2 infection, followed by nasal delivery of isotype control or anti-CD3 antibody for 4 weeks. **(B)** Representative confocal images and quantification of IBA1+ microglia in subcortical white matter and dentate gyrus from mock mice, mild COVID mice treated with isotype control or anti-CD3; n=5 mice per group. **(C)** Representative confocal images and quantification of GFAP+ astrocytes in the same regions and groups; n = 5 mice per group. Scale bars, 100µm. **(D)** Serum level of CXCL10 and IL-10 in mock, mild COVID + isotype and mild COVID + anti-CD3 groups; n=4-5 mice per group. Data are mean ± SEM; each dot represents an individual mouse. *p <0.05, ** p <0.01, ***p <0.001, ****p <0.0001 (one way ANOVA followed by Tukey's multiple comparison test).

Figure 2

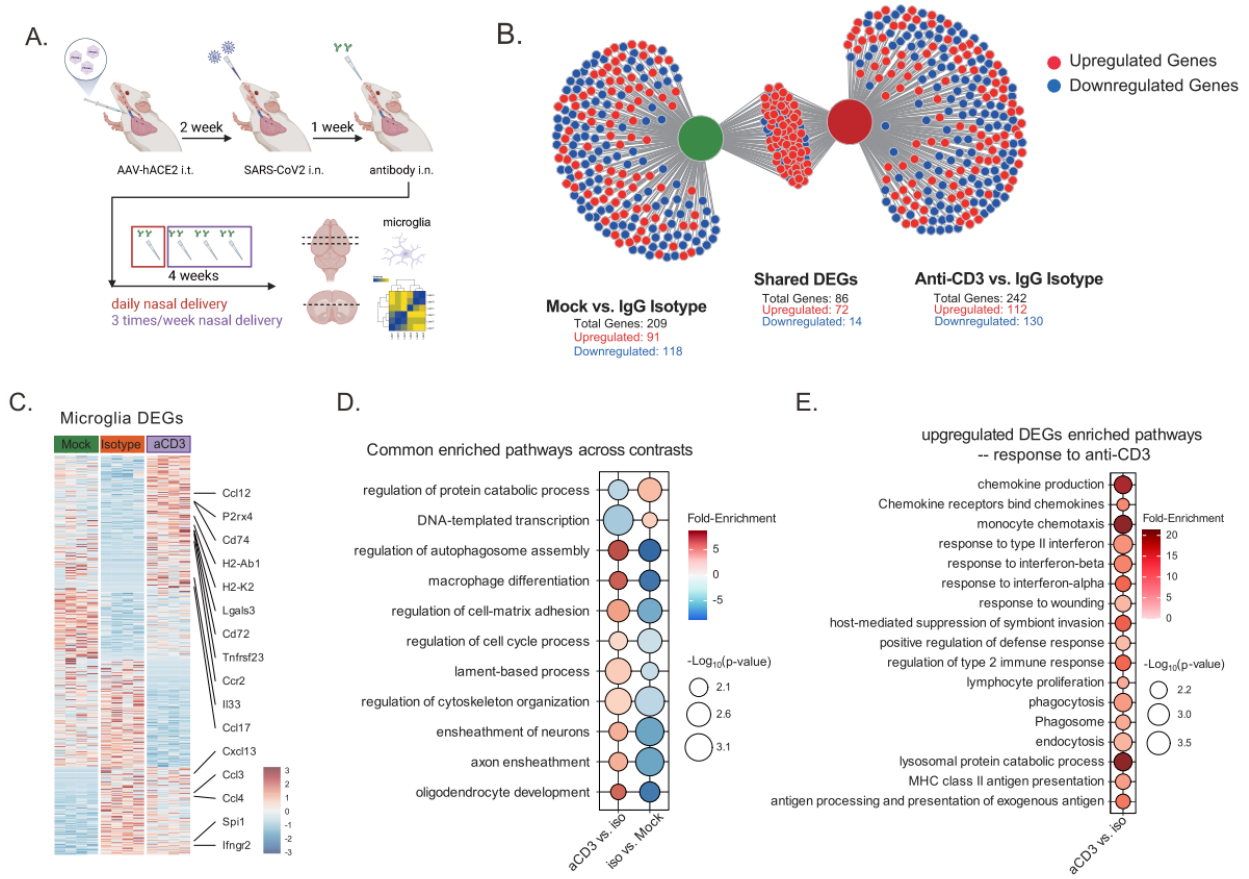

Figure. 2 Nasal anti-CD3 treatment reprograms microglial transcriptional states in mild COVID (A) Experimental paradigm for bulk RNA-seq of subcortical microglia from mock infected mice and mild COVID mice treated with isotype control or nasal anti-CD3. **(B)** Network plot showing overlap of differentially expressed genes (DEGs) in microglia from isotype treated mild COVID versus mock and anti CD3–treated mild COVID versus isotype; shared DEGs represent genes differentially expressed in both contrasts (associated Fig S1D). **(C)** Heatmap of microglial DEGs identified in either comparison (mock vs isotype or anti-CD vs isotype), n=4-5 mice per group. Selected genes associated with antigen presentation and chemokine signaling are highlighted. **(D)** Gene ontology (GO) categories enriched among cross comparison DEGs, illustrating pathways most consistently modulated by infection and treatment. **(E)** GO pathways enriched among genes upregulated in anti-CD3 treated versus isotype treated mild COVID microglia.

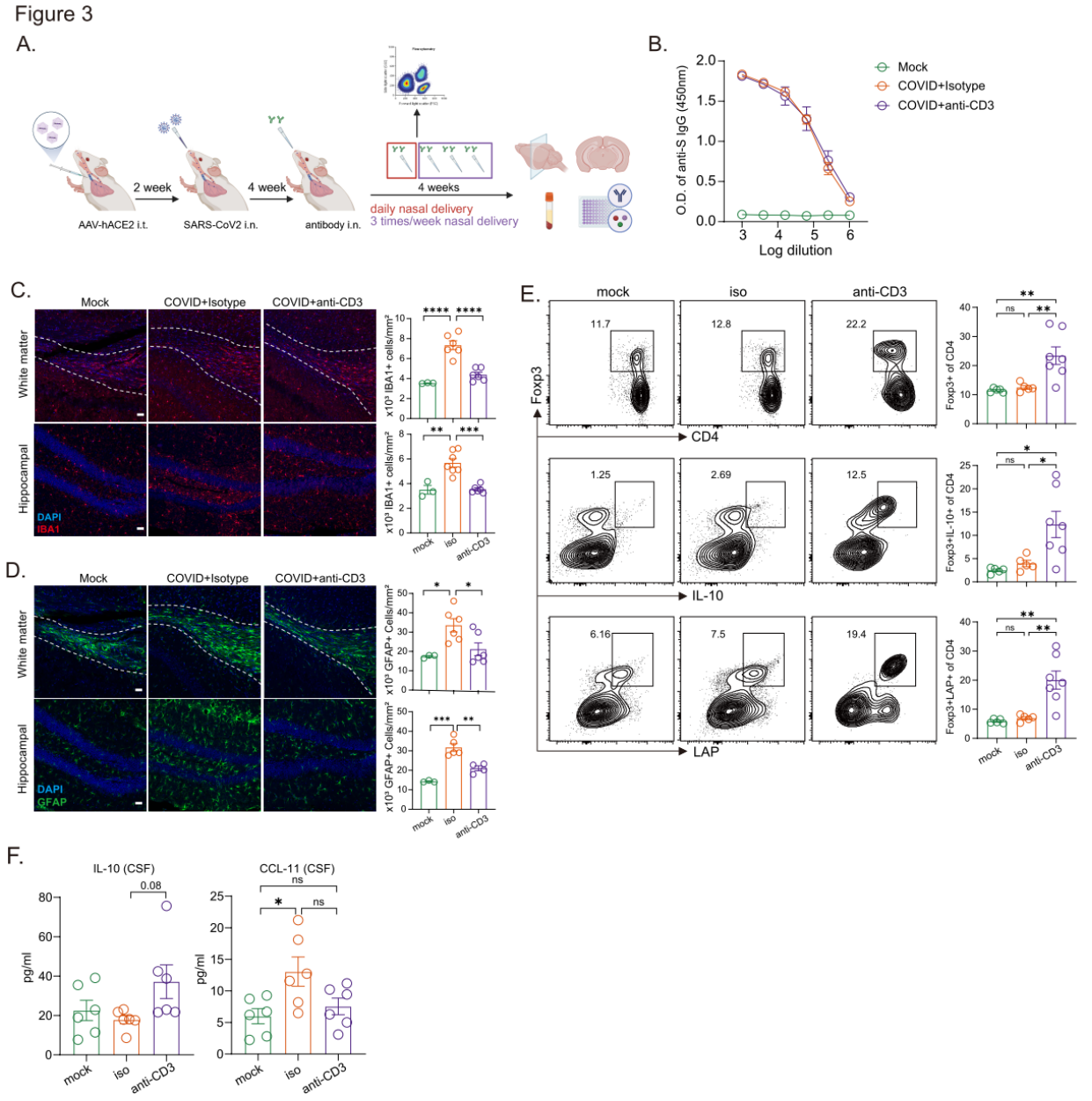

Figure. 3 Nasal anti-CD3 induces brain Treg cells and reverses persistent neuroinflammation in mild COVID. (A) Experimental paradigm for delayed intranasal anti-CD3 treatment in the mild COVID mouse model. **(B)** Serum anti-spike IgG titers measured by ELISA, n=6-7 mice per group. **(C)** Representative confocal images and quantification of IBA1+ microglia in subcortical white matter and dentate gyrus from mock, mild COVID + isotype and mild COVID + aCD3 mice; n = 3–7 mice per group. **(D)** Representative confocal images and quantification of GFAP+ astrocytes in the same regions and groups; n=3-7 mice per group. Scale bars, 100μm. **(E)** Representative flow cytometry plots and quantification of Foxp3+, Foxp3+IL-10+, and Foxp3+LAP+ CD4 T cells (gated on live CD45+CD11b-TCRβ+CD4+) in brain tissue. **(F)** Cerebrospinal fluid (CSF)

813 concentrations of IL-10 and CCL-11 in mock, mild COVID + isotype or anti-CD3 groups; n=6-7
814 mice per group. Data are mean ± SEM; each dot represents an individual mouse. *p <0.05, ** p
815 <0.01, ***p <0.001, ****p <0.0001 (one way ANOVA followed by Tukey's multiple comparison
816 test).

Figure 4

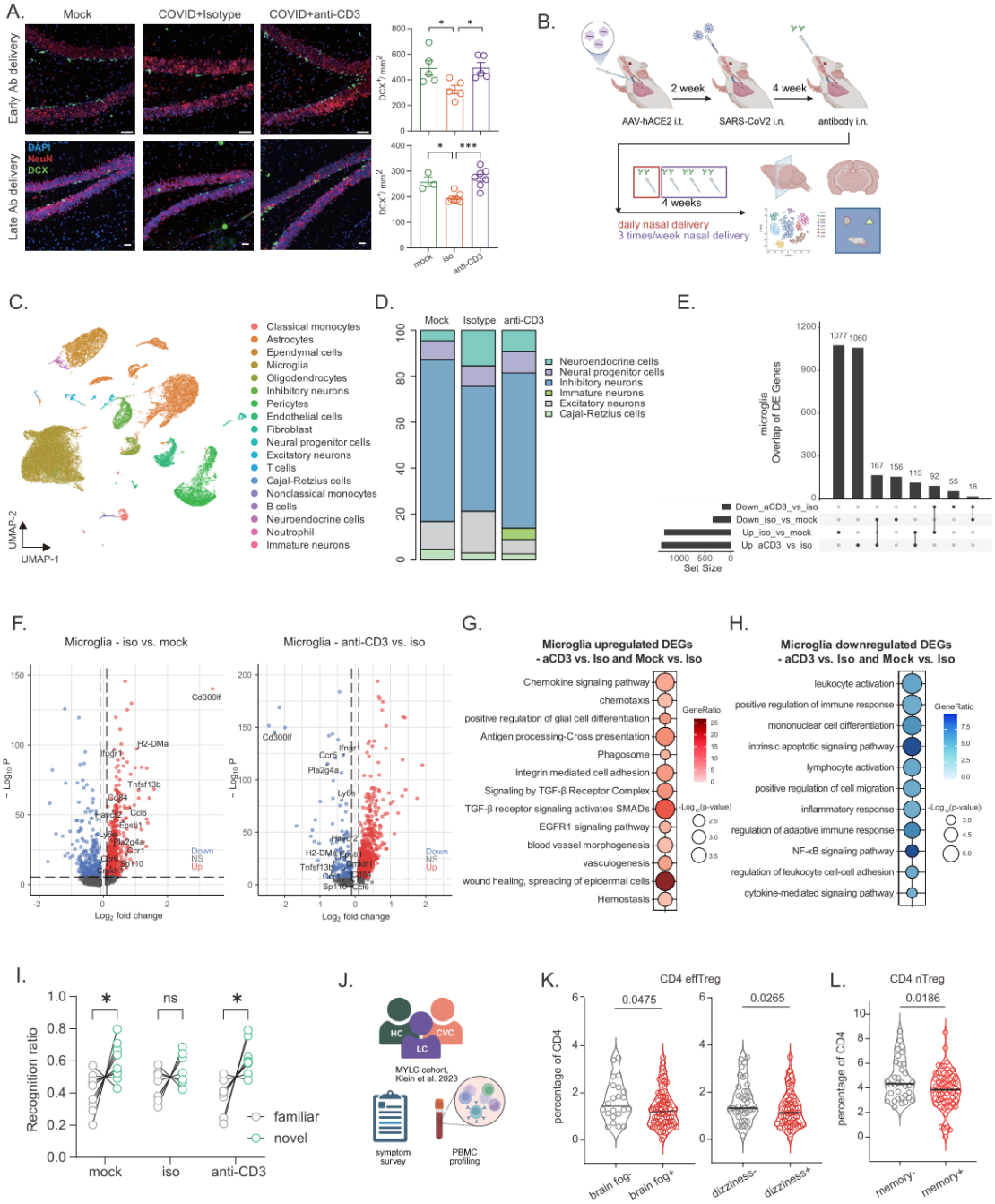

Figure. 4 Nasal anti-CD3 antibody treatment improves neurogenesis and associated cognitive function in mild COVID mouse model. (A) Quantification and confocal micrograph of neuroblast (DCX+) in the dentate after 4 weeks anti-CD3 antibody administration in mild COVID or mock mice. Scale bars, 100μm (early) or 50μm (late). Data shown as mean ± SEM; each dot represents an individual mouse; analyzed by one way ANOVA followed by Tukey's multiple comparison test. **(B)** Schematic of experimental paradigm for nasal anti-CD3 antibody

824 administration to treat neuroinflammation in mild COVID mouse model. **(C)** Uniform manifold
825 approximation and projection (UMAP) of scRNA-seq data in brain parenchyma cells enriched
826 from subcortex region. **(D)** Distribution of different neuron subsets from the scRNAseq. **(E)** Upset
827 plot comparing the microglia DEGs. **(F)** Volcano plot illustrating results of differential expression
828 testing between microglia from iso compared with mock or anti-CD3. **(G-H)** GO pathways
829 analysis comparing microglia DEGs between iso and mock or anti-CD3. **(I)** Quantified recognition
830 ratio from novel objection recognition testing in 4 weeks antibody treated mild COVID or mock
831 mice. **(J)** Schematic of the MY-LC study. **(K)** Percentage of circulating effector Treg cell and **(I)**
832 nTreg in Long COVID patients with and without indicated symptoms. ns=no significant difference,
833 *p <0.05, ** p <0.01, ***p <0.001, ****p <0.0001.

Figure S1

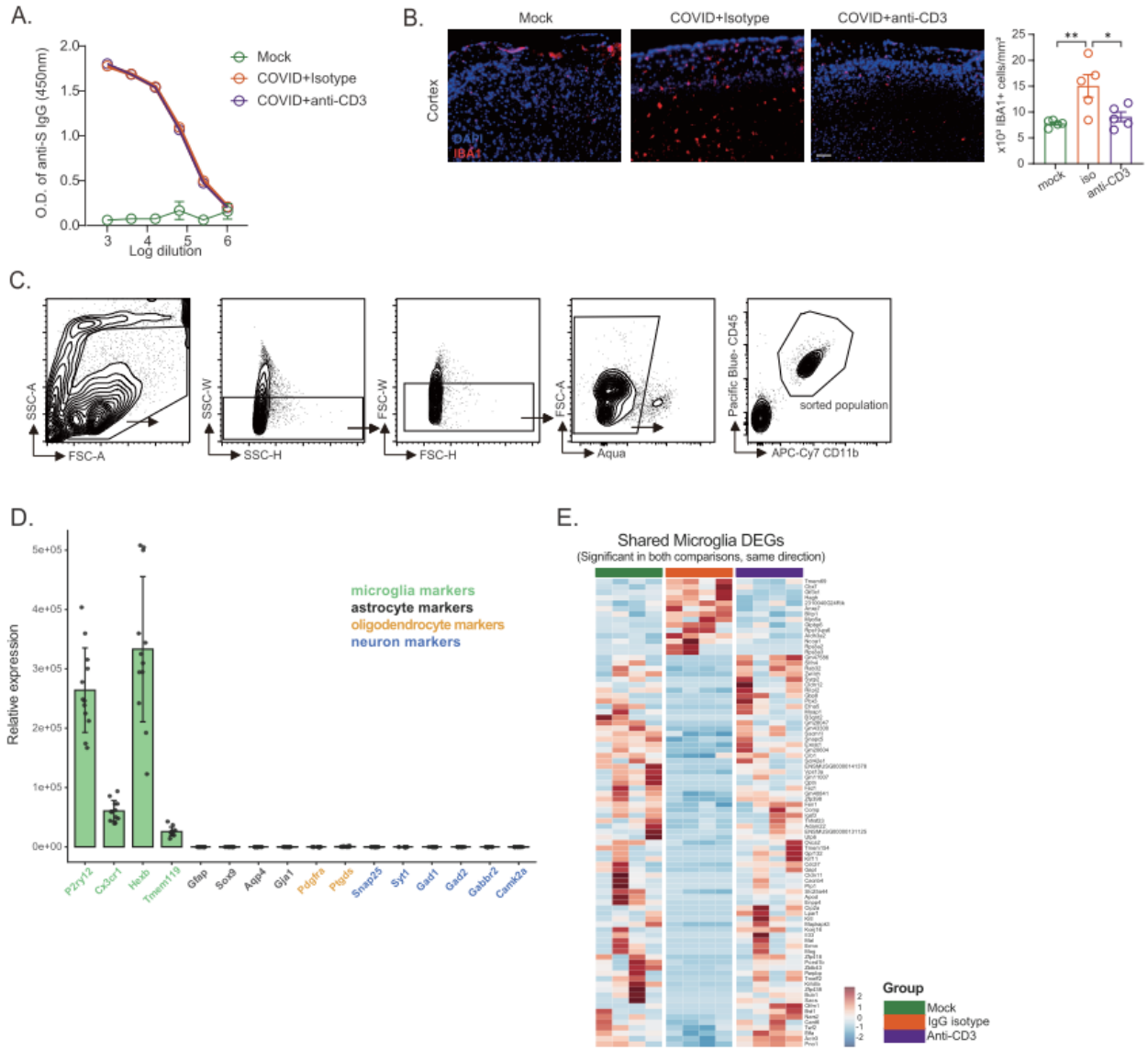

Figure. S1 Additional data of early nasal anti-CD3 treatment in mild COVID mice, related to Figure1 & 2. (A) Serum antibodies were measured against spike protein using an ELISA, n=6-7 mice per group. **(B)** Quantification and confocal micrograph of microglia (IBA1+) in the cortex after 4 weeks isotype or anti-CD3 antibody administration in mild COVID or mock mice; n=6-7 mice per group. Data shown as mean ± SEM; each dot represents an individual mouse. *p <0.05, ** p <0.01, ***p <0.001, ****p <0.0001 (one way ANOVA followed by Tukey's multiple comparison test). **(C)** Representative gating strategy to isolate microglia for bulk RNAseq. **(D)** Relative expression of cell type-specific markers in sorted microglia. **(E)** Heatmap of shared microglial DEGs significant in both comparisons (Mock vs IgG isotype and anti-CD3 vs IgG isotype) and changing in the same direction. n=4 or 5 mice per group.

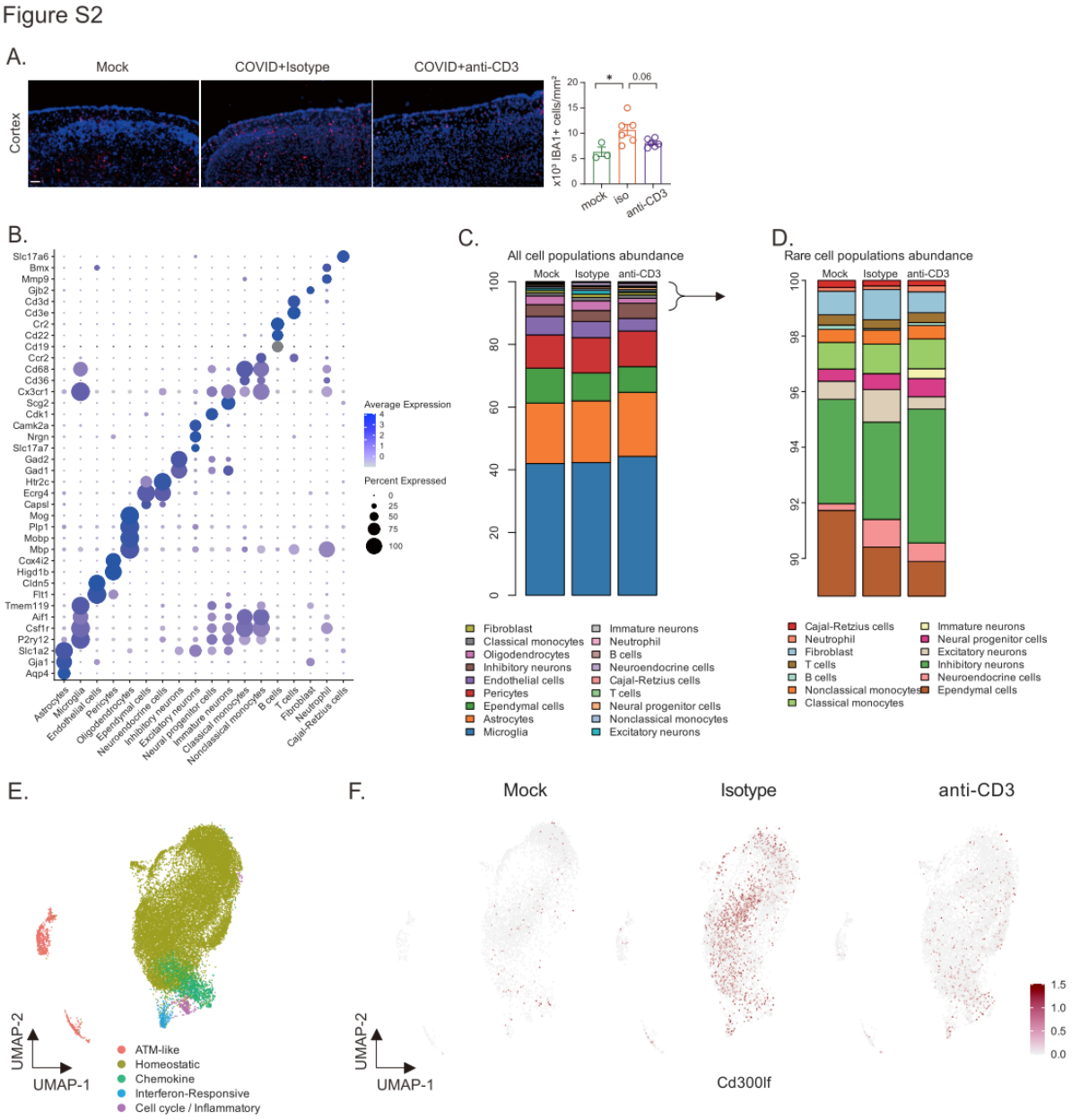

Figure. S2 Additional data of late nasal anti-CD3 treatment in mild COVID mice, related to Figure3 & 4. (A) Quantification and confocal micrograph of microglia (IBA1+, red) in the cortex after 4 weeks isotype or anti-CD3 antibody administration in mild COVID or mock mice; n=3-7 mice per group. Data shown as mean ± SEM; each dot represents an individual mouse. *p <0.05, ** p <0.01, ***p <0.001, ****p <0.0001 (one way ANOVA followed by Tukey's multiple comparison test) .**(B)** Dot plot showing expression of cell type marker genes used in the annotation the clusters shown in figure 4C and 4D. **(C)** Distribution of total cell subsets in the scRNAseq and **(D)** distribution of the least abundant cell types. **(E)** UMAP plot of microglia

856 colored by clusters. **(F)** UMAP plots as in (E) colored by expression level of Cd300lf.